Side-On Bridging Coordination of N_2: Spectroscopic Characterization of the Planar Zr_2N_2 Core and Theoretical Investigation of Its Butterfly Distortion

Felix Studt,[a] Lara Morello,[b] Nicolai Lehnert,[a] Michael D. Fryzuk,[b] and Felix Tuczek*[a]

Abstract: The vibrational and electronic structure of the side-on N_2-bridged Zr complex $[\{(P_2N_2)Zr\}_2(\mu\text{-}\eta^2\text{:}\eta^2\text{-}N_2)]$ ($P_2N_2 = PhP(CH_2SiMe_2NSiMe_2CH_2)_2PPh$) were analyzed. The vibrational characterization of the planar Zr_2N_2 core was based on resonance Raman and infrared spectroscopy. In the Raman spectrum, the N–N stretching band is found at 775 cm^{-1} with an isotope shift of 22 cm^{-1}. Due to its appearance in many overtones and combination modes, the metal–metal stretch is assigned to the peak at 295 cm^{-1}. The two ungerade modes of the Zr_2N_2 core were identified in the infrared spectrum. Based on these four vibrations of the Zr_2N_2 unit, a quantum chemical assisted normal coordinate analysis (QCA-NCA) was performed. The force constants for the N–N and Zr–N bonds were calculated to be 1.53 and 2.58 mdyn $Å^{-1}$, respectively. The butterfly distortion of the Zr_2N_2 unit obtained in DFT geometry optimizations of planar side-on N_2-bridged Zr complexes was analyzed in more detail. It was found that on bending of the Zr_2N_2 core, the lone pairs of the axial amide ligands are rotated by 90°. The bent Zr_2N_2 unit is 11 kcal mol^{-1} lower in energy than the planar core due to a more uniform distribution of electron density between the metal atoms and N_2 and delocalization of electron density from the amide ligands to the Zr_2N_2 unit. The spectroscopic implications of this distortion are analyzed.

Keywords: coordination modes · dinitrogen complexes · nitrogen · vibrational spectroscopy · zirconium

Introduction

The activation of molecular nitrogen (N_2) by transition metal complexes is experiencing renewed interest and growth.[1] The extent to which the dinitrogen ligand is activated can be determined by consideration of N–N bond lengths from X-ray diffraction data and N–N stretching frequencies obtained by Raman and IR spectroscopy. These data allow dinitrogen complexes to be divided into weakly, moderately and highly activated,[2] whereby the last-named category has the longest N–N bonds and lowest N–N stretching frequencies. Complexes in this group generally have early transition metals stabilized by strongly electron-donating ancillary ligands, and in all of them the dinitrogen unit bridges two metal centers in a variety of modes. The end-on bridging mode is the most common, with N–N bond lengths in the range 1.2–1.3 Å and stretching frequencies of approximately 1200–1300 cm^{-1}.[3] The side-on bridging mode of coordination produces highly activated N_2 units, as evidenced by N–N bond lengths of approximately 1.5 Å and N–N stretching frequencies of 700–800 cm^{-1};[3–5] these complexes can be formally described as containing the highly reduced hydrazido(4 –) unit. Somewhat less common is the edge-on bridging mode, which in one case showed an N–N bond length of 1.4 Å and a stretching frequency of 850 cm^{-1}.[6, 7]

Not all complexes that contain side-on bridging dinitrogen display a highly activated N_2 unit. Dinuclear side-on N_2 complexes of the lanthanides and actinides range from only slightly activated (N–N 1.0–1.1 Å)[8–11] to moderately activated (N–N 1.23 and 1.26 Å, respectively);[12, 13] a dinuclear ansazirconocene complex also contains a moderately activated side-on dinitrogen ligand (N–N 1.24 Å).[14]

Dinuclear zirconium complexes with side-on bridging dinitrogen units and stabilizing amidophosphine-type ancillary ligands have been studied extensively with regard to their structural parameters and reactivity.[15–17] The series of complexes $[\{(PNP)ZrCl\}_2(\mu\text{-}\eta^2\text{:}\eta^2\text{-}N_2)]$ (**1**), $[\{(PNP)Zr(OAr)\}_2(\mu\text{-}\eta^2\text{:}\eta^2\text{-}N_2)]$ (**2**; $PNP = N(SiMe_2CH_2PiPr_2)_2$, $OAr = O\text{-}2,6\text{-}Me_2C_6H_3$), and $[\{(P_2N_2)Zr\}_2(\mu\text{-}\eta^2\text{:}\eta^2\text{-}N_2)]$ (**3**; $P_2N_2 = PhP(CH_2SiMe_2NSiMe_2CH_2)_2PPh$) have N–N bond lengths in range of 1.43–1.54 Å (see Scheme 1). In addition, all of these complexes are intensely blue or blue-green as a result of a charge-transfer absorption around 650 nm. For **1** and **2**, resonance Raman spectroscopy confirmed the highly activated nature of dinitrogen unit, although in neither case were IR

[a] Prof. F. Tuczek, F. Studt, Dr. N. Lehnert
Institut für Anorganische Chemie
Christian Albrechts Universität Kiel
Ohlshausenstrasse 40, 24098 Kiel (Germany)

[b] L. Morello, Prof. M. D. Fryzuk
Department of Chemistry
University of British Columbia, Vancouver
Vancouver, BC V6T 1Z1 (Canada)
E-mail: ftuczek@ac.uni-kiel.de

0947-6539/03/0902-0520 $ 20.00+.50/0 *Chem. Eur. J.* **2003**, *9*, No. 2

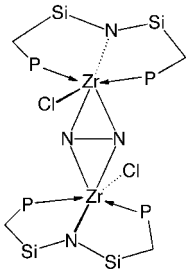

1

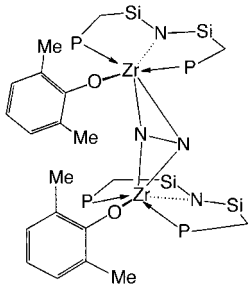

2

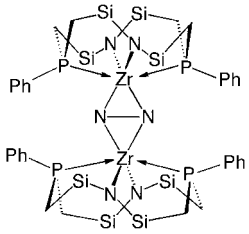

3

Scheme 1. All methyl groups on the Si atoms and isopropyl groups on the P atoms have been omitted for clarity.

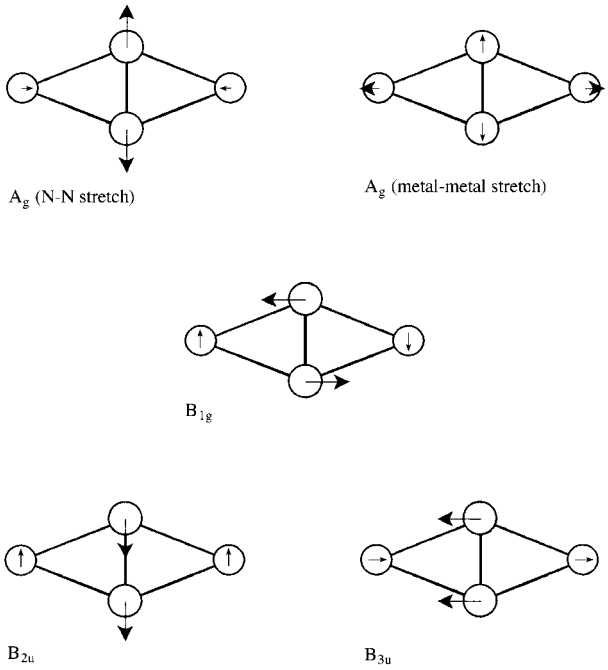

Figure 1. Eigenvectors for the five in-plane modes of the Zr_2N_2 core. The arrows correspond to unit displacements of normal coordinates with a scaling factor of two.

data measured.[3, 5] Here we report detailed IR and Raman studies and DFT calculations on the macrocyclic complex **3**. The vibrational data were complemented by isotopic substitution with $^{15}N_2$ and evaluated by quantum chemistry assisted normal coordinate analysis (QCA-NCA), which was developed earlier to account for the vibrational properties of mononuclear dinitrogen complexes of Mo and W.[18] Based on the ab initio electronic structure description of **3**, the electronic transitions of the $Zr_2(\mu\text{-}\eta^2\text{:}\eta^2\text{-}N_2)$ core can be assigned. Finally, the bending of the $Zr_2(\mu\text{-}\eta^2\text{:}\eta^2\text{-}N_2)$ unit was investigated from the point of view of electronic structure, and the influence of butterfly distortion on the electronic and vibrational spectroscopic properties of this core was analyzed.

Results and Analysis

Vibrational spectroscopy: The planar Zr_2N_2 core (D_{2h} symmetry) has five in-plane normal modes (Figure 1), three of which are Raman-active ($2 \times A_g$ and B_{1g}) and two of which are IR-active (B_{2u} and B_{3u}).[19] Solid-state resonance Raman spectra of **3** and its $^{15}N_2$ isotopomer, recorded at an excitation wavelength of 647.1 nm, are shown in Figure 2. Raman spectra of **3** were also recorded at other wavelengths (data not shown), but at 647.1 nm the resonance enhancement of the vibrational modes of the Zr_2N_2 core was at its maximum. Moreover, these spectra exhibit a wealth of overtones and combination modes. The most intense peaks are located at 295 and 775 cm^{-1}. In the spectrum of the ^{15}N isotopomer the 775 cm^{-1} peak shifts by -22 to 753 cm^{-1}, whereas the 295 cm^{-1} peak has a very small shift of about 1 cm^{-1}. Based on the magnitude of its isotope shift, the 775 cm^{-1} peak is assigned to the N–N stretching mode of the Zr_2N_2 core, which has A_g symmetry in the D_{2h} point group. In addition, there are less intense peaks at 239, 268, 342, 394 and 442 cm^{-1} which show no isotope sensitivity. These features are designated as A–E (see Table 1 and Figure 2). All other peaks in the spectra are overtones and combination modes of peaks A–E with the 295 and 775 cm^{-1} vibrations (designated X and Y, respectively) or overtones and combination modes of X and Y themselves. Based on these findings and the DFT results (see below), the 295 cm^{-1} peak X is assigned to the metal–metal stretch, which also has A_g symmetry in the D_{2h} point group.

The complete experimental spectral range shows clusters of overtones and combination modes (see Figure 2). The peaks between 534 and 739 cm^{-1} can be assigned to combinations of the metal–metal stretch X with modes A–E. The peak at 589 cm^{-1} is the first overtone of the metal–metal stretch (2X). Remarkably, the combination mode of X and E at 739 cm^{-1} is more intense than the fundamental mode E due to its small energetic separation to the N–N stretching mode (Fermi resonance). This effect increases in the spectrum of the isotopically labelled compound because the energetic separation between E + X (737 cm^{-1}) and the N–N stretch (753 cm^{-1}) becomes even smaller. The combination modes of A–D with the first overtone of the metal–metal stretch (2X) lie in the range 829–984 cm^{-1}. The peaks between 1014 and 1218 cm^{-1} (995 and 1147 cm^{-1} for the ^{15}N-labelled compound) are assigned to combinations of the N–N stretching mode with A–E. In the ^{15}N spectrum this region further contains combinations of B–D with the intense peak X+E (737 cm^{-1}, see above). The peaks from 1310 to 1513 cm^{-1} (1287 to 1441 cm^{-1} for the ^{15}N-labelled compound) are assigned to combinations of X+Y with modes A–E, whereas the peak at 1366 cm^{-1} (1343 cm^{-1} for the ^{15}N-labelled compound) corresponds to the combination of the N–N

  0947-6539/03/0902-0521 $ 20.00+.50/0

Table 1. Fundamental and combination modes observed in the Raman spectra in Figure 2.

Mode[a]	Frequency [cm^{-1}]		Mode[a]	Frequency [cm^{-1}]		Mode[a]	Frequency [cm^{-1}]	
	^{14}N	^{15}N		^{14}N	^{15}N		^{14}N	^{15}N
A	239	239	Y	775	753	Y+C	1117	1096
B	268	268	2X+A	829	829	X+E+D	–	1230
X	295	294	2X+B	855	854	Y+D	1169	1147
C	342	342	3X	882	880	Y+E	1218	–
D	394	394	2X+C	931	930	Y+X+A	1310	1287
E	442	442	2X+D	984	984	Y+X+B	1338	1317
X+A	534	533	Y+A	1014	995	Y+2X	1366	1343
X+B	562	562	X+E+B	–	1005	Y+X+C	1414	1390
2X	589	588	Y+B	1043	1021	Y+X+D	1466	1441
X+C	636	635	X+E+X	–	1032	Y+X+E	1513	–
X+D	688	687	Y+X	1070	1048	2Y	1541	1486
X+E	739	737	X+E+C	–	1079			

[a] X is assigned to the metal–metal stretch and Y to the N–N stretch.

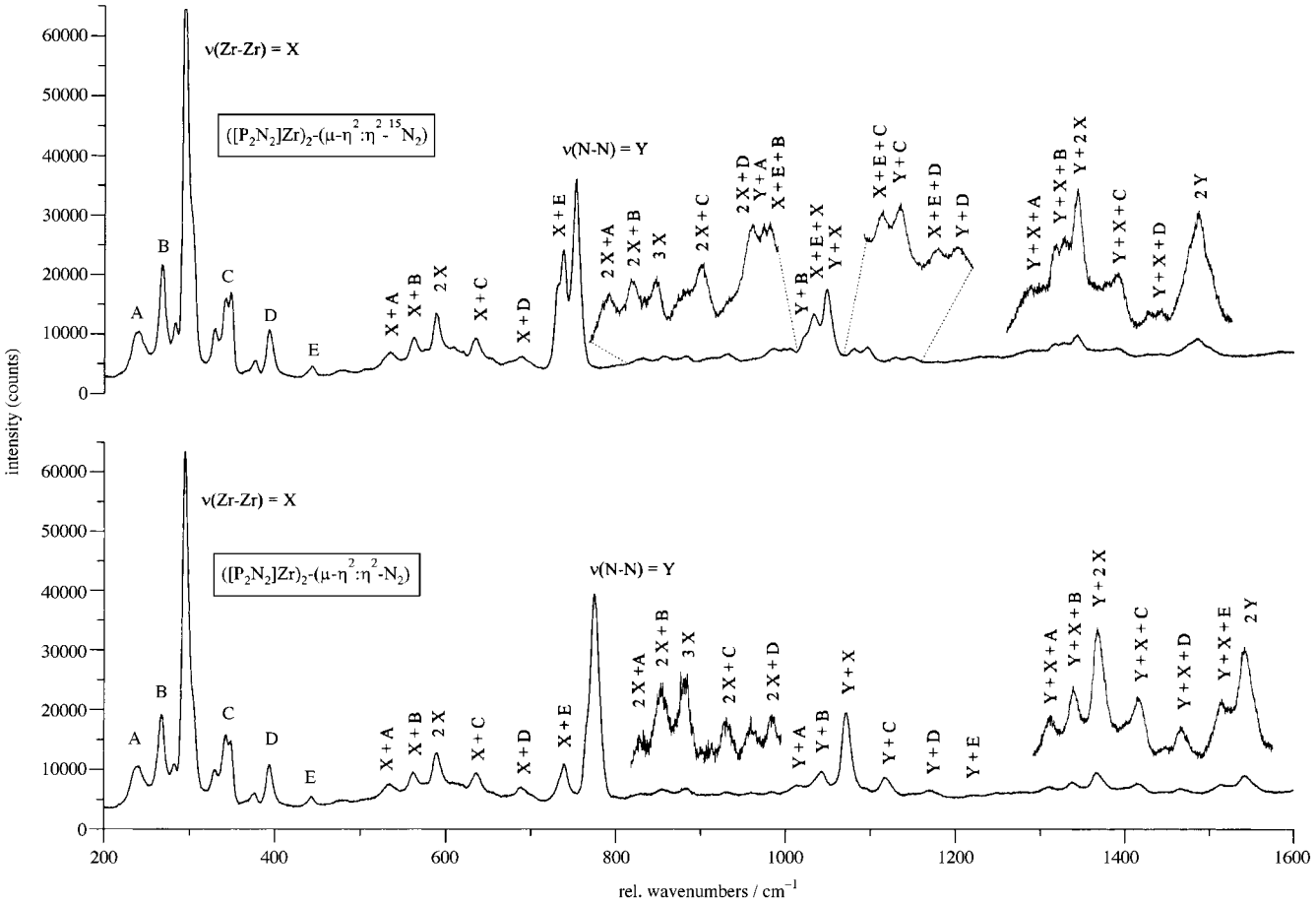

Figure 2. Raman spectra of complex **3** recorded with an excitation wavelength of 674.1 nm at 10 K. Bottom: unlabelled complex. Top: ^{15}N-labelled compound.

stretch with the first overtone of the metal–metal stretch. The peak at 1541 cm^{-1}, which has an isotope shift of 55 cm^{-1}, can be assigned to the first overtone of the N–N stretch.

So far, two of the three Raman active vibrations have been identified and correspond to the two A_g modes (N–N stretch and metal–metal stretch). Based on DFT calculations and normal coordinate analysis (see below), the third Raman active mode ν(ZrN) of B_{1g} symmetry should have a frequency of 600–700 cm^{-1} and an isotope shift of about 20 cm^{-1}. No such feature is observed in the Raman spectra. The absence of a peak corresponding to this vibration in the planar structure and its appearance in the bent structure are analyzed below. To obtain information on the ungerade vibrations of the planar Zr_2N_2 core, infrared spectra of **3** were recorded. Figure 3 shows the middle (MIR) and far infrared (FIR) spectra of **3** and its ^{15}N isotopomer. The region below 700 cm^{-1} exhibits an intense band at 690 cm^{-1} in the ^{14}N spectrum which shifts to a broad feature having two components at 684 and 680 cm^{-1} in the ^{15}N spectrum. Based on the calculations and the NCA these shifts must be attributed to the B_{3u} vibration, which itself should

0947-6539/03/0902-0522 $ 20.00+.50/0 *Chem. Eur. J.* **2003**, *9*, No. 2

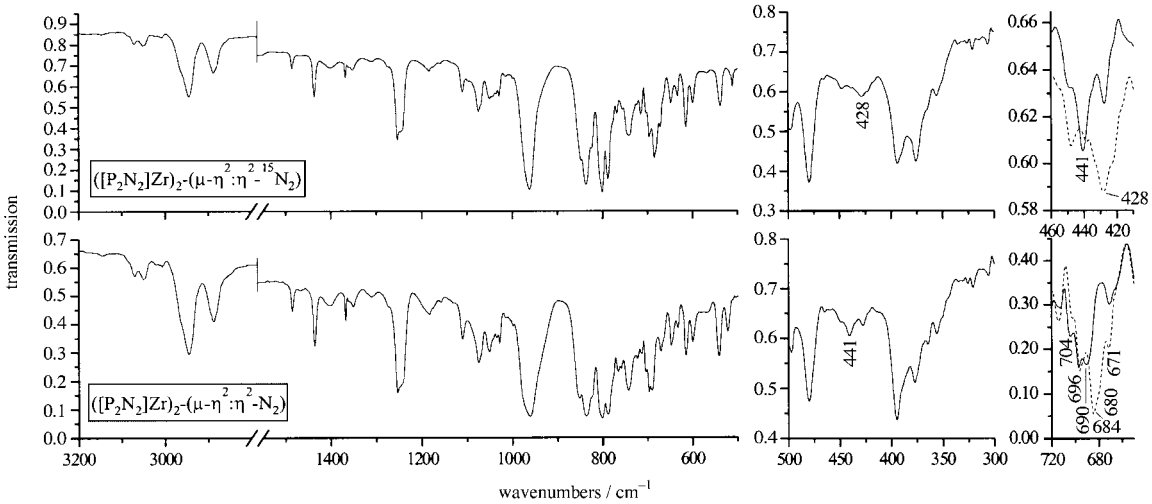

Figure 3. IR spectra of complex **3** at 10 K. Bottom: unlabelled complex. Top: ^{15}N-labelled compound. Detail plots in the region between 720 and 650 cm^{-1} and from 460 to 410 cm^{-1}.

exhibit a ^{15}N isotope shift of about 20 cm^{-1}. Inspection of the spectra shows that this shift is clearly distributed over at least one additional vibration, which could be a terminal ligand mode that mixes with the B_{3u} vibration. In the region from 450 to 420 cm^{-1} a shift of the band at 441 to 428 cm^{-1} is observed. This must be associated with the B_{2u} mode, which is calculated to be located in this region (see below).

UV/Vis spectroscopy: The UV/Vis spectrum of complex **3** (Figure 4) exhibits a characteristic absorption band at 670 nm. Based on the high intensity of this band, it is assigned to a charge-transfer (CT) transition from the ligand orbitals into

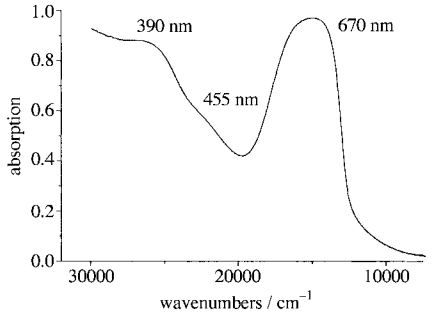

Figure 4. UV/Vis spectrum of **3** at 10 K.

the empty d orbital manifold of the metal centers. As there is no CT band of lower energy, the 670 nm band is assigned to the lowest energy CT transition of **3**, which, based on the MO scheme in Figure 5, corresponds to the electric-dipole allowed transition $\pi^*_{v\_}\, d^+_{yz} \rightarrow d^-_{yz}$, that is, the HOMO–LUMO transition (for the nomenclature of the orbitals, see below). Since the HOMO $\pi^*_{v\_}\, d^+_{yz}$ ($b_{3g}\langle 53\rangle$) has 65% nitrogen contribution, and the LUMO d^-_{yz} ($a_u\langle 54\rangle$) has 56% zirconium d character, this feature corresponds to an $N_2 \rightarrow Zr$ LMCT transition. This CT excited state should exhibit shortening of the N–N bond (removal of an electron from π^*_v) and lengthening of Zr–N distance (transfer of an electron from a N_2–metal bonding to a nonbonding orbital). Based on the Albrecht A-term

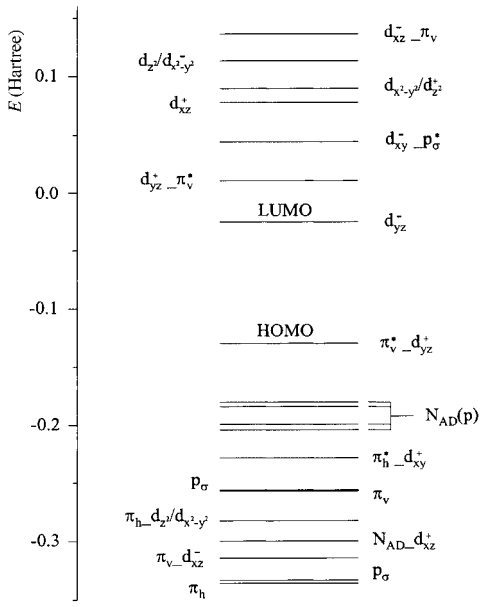

Figure 5. MO diagram of model **I**. MO designations correspond to those in Table 7.

mechanism,[20, 21] this would enhance both A_g vibrations of the Zr_2N_2 core, in agreement with the resonance enhancement for the N–N and metal–metal stretching vibrations observed on irradiation at 647.1 nm (see above). Two additional absorption bands at 455 and 390 nm are assigned to transitions from the HOMO $\pi^*_{v\_}\, d^+_{yz}$ to higher energy zirconium d orbitals.

Normal coordinate analysis: The QCA-NCA procedure was performed as described in the Experimental Section. For the DFT determination of the theoretical force field, model **I** with D_{2h} symmetry was used. In the course of the QCA-NCA procedure the hydrogen atoms of the PH_3 and NH_2 ligands of model **I** were removed to give simplified model **Ia** (Figure 6). Since only the vibrational modes of the Zr_2N_2 core are of interest, only the force constants of the Zr_2N_2 unit were fitted. The four Zr–N (r_1–r_4) and the N–N (r_{NN}) distances were used as internal coordinates (Figure 7). The bond lengths and

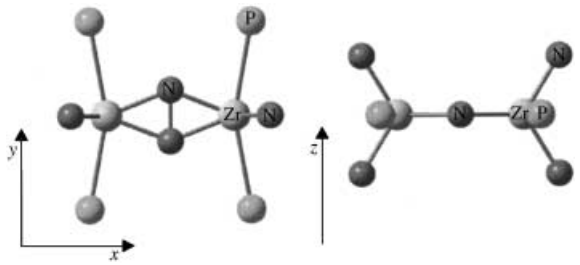

Figure 6. Model **Ia** used for QCA-NCA calculation.

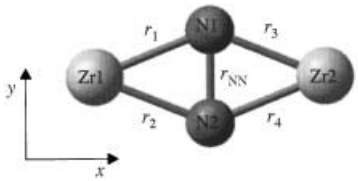

Figure 7. Internal coordinates and atomic labeling chart for model **I**.

angles of the N and P terminal ligands and the corresponding force constants were fixed at their values from the DFT calculation. Due to the high symmetry of the Zr_2N_2 core, all diagonal r_ir_i interaction matrix elements have the same value. Furthermore, two off-diagonal elements of the r_ir_j interaction and the off-diagonal element of the r_ir_{NN} interaction were included in the NCA, whereas one off-diagonal element of the r_ir_j interaction was set to zero because its value is small. The resulting f matrix is shown in Equation (1).

	r_1	r_2	r_3	r_4	r_{NN}
r_1	x	a	b	0	c
r_2	a	x	0	b	c
r_3	b	0	x	a	c
r_4	0	b	a	x	c
r_{NN}	c	c	c	c	y

(1)

Symmetry adaption of the internal coordinates of the Zr_2N_2 core leads to five symmetry coordinates [Eq. (2)]. Two of

$$S_1^{A_g} = \frac{1}{2}(r_1 + r_2 + r_3 + r_4)$$

$$S_2^{A_g} = r_{NN}$$

$$S_1^{B_{1g}} = \frac{1}{2}(r_1 - r_2 - r_3 + r_4) \quad (2)$$

$$S_1^{B_{2u}} = \frac{1}{2}(r_1 - r_2 + r_3 - r_4)$$

$$S_1^{B_{3u}} = \frac{1}{2}(r_1 + r_2 - r_3 - r_4)$$

them have A_g symmetry, and the others are of B_{1g}, B_{2u} and B_{3u} symmetry. As discussed above, the two A_g modes were found in the Raman spectrum, and the B_{2u} and B_{3u} modes in the IR data. The B_{1g} mode was not observable in the spectra.

The relevant F matrix for the Zr_2N_2 core is shown in Equation (3). The five different force constants were fitted to the experimental data. The resulting eigenvectors (normal modes) are shown in Figure 1.

$A_g^{(1)}$	$A_g^{(2)}$	$B_{1g}^{(1)}$	$B_{2u}^{(1)}$	$B_{3u}^{(1)}$
$x+a+b$	$2c$	0	0	0
$2c$	y	0	0	0
0	0	$x-a-b$	0	0
0	0	0	$x-a+b$	0
0	0	0	0	$x+a-b$

(3)

Table 2 compares the experimentally determined frequencies, the calculated data from DFT calculations (B3LYP) and the QCA-NCA results. The agreement between the DFT frequencies and the experiment is fair: The N–N stretch is found at 775 cm^{-1} with an isotope shift of 22 cm^{-1} and is calculated to be at 717 cm^{-1}, with the same isotope shift. The metal–metal stretch is calculated by DFT to be at 262 cm^{-1} and is found at 295 cm^{-1}. The B_{1g} mode is not observed in the spectra. From the DFT calculations this vibration is predicted to be at 685 cm^{-1} with an isotope shift of 18 cm^{-1}. The infrared-active B_{3u} mode at 690 cm^{-1} is calculated to be at 780 cm^{-1}. For the B_{2u} mode only one band at 441 cm^{-1} is observed, whereas the DFT calculation indicates splitting into two bands at 403 and 313 cm^{-1}.

Table 2. Comparison of the observed and calculated frequencies of complex **3** with model system **I**.

Mode	Experimental		QCA-NCA		B3LYP	
	^{14}N [cm^{-1}]	^{15}N [cm^{-1}]	^{14}N [cm^{-1}]	^{15}N [cm^{-1}]	^{14}N [cm^{-1}]	^{15}N [cm^{-1}]
$A_g(1)$	295[a]	294[a]	295	294	262	261
$A_g(2)$	775[a]	753[a]	776	752	717	695
B_{1g}	n.o.	n.o.	628	609	685	667
B_{2u}	441	428	440	429	403	397
					313	310
B_{3u}	690	684	696	676	780	757
		680				

[a] Raman data; unlabelled data is IR data; n.o. = not observed.

Comparison of the experimental data and the QCA-NCA results shows good agreement (Table 2). The B_{1g} mode is not found in the spectra and is predicted by QCA-NCA to be at 628 cm^{-1}. The force field obtained for the Zr_2N_2 core is given in Table 3. The force constant of the N–N stretch is 1.53 mdyn $Å^{-1}$. This reflects the extreme activation of dinitrogen in the complex compared to the free N_2 molecule (22.42 mdyn $Å^{-1}$).[22] In fact, this force constant is even lower than that of free hydrazine (4.3 mdyn $Å^{-1}$).[23] The force constant of the Zr–N stretch between zirconium and N_2 is 2.58 mdyn $Å^{-1}$.

Table 3. Force constants of the internal coordinates of the Zr_2N_2 core.

Internal coordinate	Force constant [mdyn $Å^{-1}$]
x	2.58
y	1.53
a	0.04
b	0.67
c	0.08

Electronic structure of the planar Zr_2N_2 core: Previous theoretical studies on the macrocyclic dinitrogen complex **3**

0947-6539/03/0902-0524 $ 20.00+.50/0 *Chem. Eur. J.* **2003**, *9*, No. 2

were carried out to better understand its reactivity with H_2 and silanes.[16] It was found that the addition of H_2 and SiH_4 across the $Zr_2(\mu\text{-}\eta^2\text{:}\eta^2\text{-}N_2)$ unit of the stripped-down model $(p_2n_2Zr)_2(\mu\text{-}\eta^2\text{:}\eta^2\text{-}N_2)$ ($p = PH_3$ and $n = NH_2$) of complex **3** is exothermic. However, these DFT calculations showed that the planar structure of this model is not the lowest energy species on the potential energy surface; instead, a bent or butterfly $Zr_2(\mu\text{-}\eta^2\text{:}\eta^2\text{-}N_2)$ core, hinged at the N–N axis, was found to be 24.4 kcal mol^{-1} more stable than the planar core in D_{2h} symmetry.[16] The origin of this butterfly distortion was tentatively attributed to an increase of orbital mixing between the Zr (4d, 5s, 5p) and dinitrogen (σ, σ*, π, π*) valence orbitals. Since the observed structure of **3** is planar in solution and in the solid state, the hypothesis put forward was that the steric bulk of the macrocyclic ligand prevented this distortion. To investigate this problem in more detail, three models of **3** having D_{2h} (**I**), C_{2v} (**II**) and C_1 (**III**) symmetry were optimized. Calculated bond lengths and angles are compared to experimental values in Table 4. The description of the electronic structure of **3** is based on the calculations on the planar model **I**.

Figure 5 shows the simplified molecular orbital diagram of **I**; contour plots and charge contributions of relevant orbitals are given in Figure 8 and Table 5, respectively. The model is oriented such that the *x* axis is along the Zr–Zr vector and the *y* axis along the N–N bond. The π_v and π_v^* orbitals of the dinitrogen ligand are vertical to the plane of the Zr-N_2-Zr unit, and the π_h and π_h^* orbitals are within this plane. The HOMO $\pi_{v\_}^*\, d_{yz}^+(b_{3g}\langle 53\rangle)$ (the superscript + indicates that both zirconium d functions have the same sign) results from the bonding combination of the π_v^* function of dinitrogen and d_{yz} to form a δ bond. This orbital has 65% nitrogen character (Table 5), which is consistent with transfer of charge from the metal atoms to dinitrogen. As the overlap between π_v^* and d_{yz} is rather small, the interaction is weak. The interaction between the π_h^* function of dinitrogen and d_{xy} is much stronger, and results in a highly covalent σ bond. The corresponding orbital $\pi_{h\_}^*\, d_{xy}^+(b_{1g}\langle 48\rangle)$ has 60% dinitrogen character (Table 5). Hence both π* functions of dinitrogen are occupied, which formally corresponds to a N_2^{4-} configuration. The LUMOs have strong participations from zirconium d orbitals; the LUMO is a pure metal d_{yz} function having no dinitrogen contribution (Table 5). For N_2 this represents an inverted bonding situation, since both backbonding π* orbitals are lower in energy than the manifold of d functions, which is empty. Importantly, the π_v and π_h orbitals of dinitrogen also strongly interact with zirconium d functions.

Table 5. Charge contributions of model **I**.[a]

Orbital	Label	Energy [Hartree]	Charge decomposition [%][b]				
			Zr	Zr d	N	P	N_{AD}[c]
$d_{xz\_}^-\pi_v$	$b_{1u}\langle 79\rangle$	0.13625	53	38	15	0	18
$d_{z^2}/d_{x^2-y^2}^-$	$b_{3u}\langle 76\rangle$	0.11337	44	31	3	13	22
$d_{x^2-y^2}/d_{z^2}^+$	$a_g\langle 75\rangle$	0.08966	50	34	3	19	8
d_{xz}^+	$b_{2g}\langle 73\rangle$	0.07774	70	30	0	10	12
$d_{xy\_}^-p_\sigma^*$	$b_{2u}\langle 66\rangle$	0.04418	47	30	9	23	0
$d_{yz\_}^+\pi_v^*$	$b_{3g}\langle 57\rangle$	0.01361	10	10	10	32	2
d_{yz}^-	$a_u\langle 54\rangle$	−0.02525	56	56	0	11	1
$\pi_{v\_}^* d_{yz}^+$	$b_{3g}\langle 53\rangle$	−0.12949	31	31	65	0	1
$N_{AD}(p)$	$b_{1u}\langle 52\rangle$	−0.17994	1	0	5	0	94
$N_{AD}(p)$	$b_{2g}\langle 51\rangle$	−0.18989	4	2	0	0	96
$N_{AD}(p)$	$b_{3u}\langle 50\rangle$	−0.19920	12	4	9	1	77
$N_{AD}(p)$	$a_g\langle 49\rangle$	−0.20406	12	7	6	3	78
$\pi_{h\_}^* d_{xy}^+$	$b_{1g}\langle 48\rangle$	−0.22831	36	32	60	1	0
p_σ	$a_g\langle 47\rangle$	−0.25574	8	3	58	26	4
π_v	$b_{1u}\langle 46\rangle$	−0.25668	13	0	50	0	34
$\pi_h d_{z^2}/d_{x^2-y^2}$	$b_{3u}\langle 45\rangle$	−0.28245	34	16	43	17	5
$N_{AD\_}d_{xz}^+$	$b_{2g}\langle 42\rangle$	−0.29976	22	12	0	0	71
$\pi_{v\_}d_{xz}^-$	$b_{1u}\langle 39\rangle$	−0.31421	22	19	19	0	53
p_σ	$a_g\langle 38\rangle$	−0.33305	10	4	14	58	8
π_h	$b_{3u}\langle 37\rangle$	−0.33554	15	1	18	40	20

[a] Only selected orbitals are listed; the superscripts in the labels of the d orbitals refer to combinations with identical (+) or opposite signs (−) of the corresponding atomic functions of the two Zr centers. [b] If several symmetry-equivalent atoms exist, the charge decomposition gives the sum of all contributions. [c] N_{AD} is the nitrogen atom of the NH_2^- group.

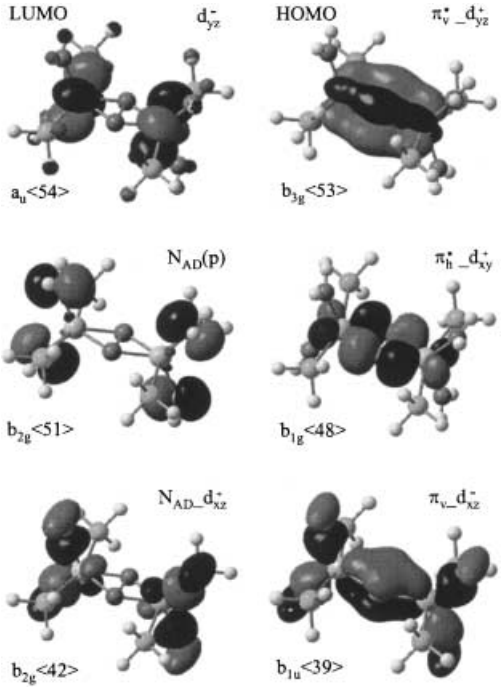

Figure 8. Contour plots of important molecular orbitals of **I**.

Table 4. Comparison of experimental and calculated structures of complex **3** with model systems **I**–**III**.

	Bond lengths [Å]					Angles [°]	Relative energies [kcal mol^{-1}][a]
	N–N	Zr–N	Zr–Zr	Zr–N_{AD}[b, c]	Zr–P[c]	Zr-N2-Zr	
X ray[15]	1.43	2.01	3.76	2.20	2.73	180	
I (D_{2h})	1.57	2.09	3.86	2.12	2.93	180	0
II (C_{2v})	1.55	2.09	3.85	2.12	2.91	164.4	−1.21
III (C_1)	1.63	2.07/2.10	3.70	2.11	2.93	147.8	−11.22

[a] Compared to model system **I**. [b] N_{AD} is the nitrogen atom of the NH_2^- group. [c] Data are averaged for simplification.

  0947-6539/03/0902-0525 $ 20.00+.50/0

Specifically, π_v interacts with the d_{xz} orbitals to form a covalent π bond (Figure 8), whereas π_h forms a combination with the $d_{z^2}/d_{x^2-y^2}$ function of the metal atoms. Since both orbitals have about 20% metal d orbital character (Table 5), this leads to a transfer of charge from dinitrogen to the zirconium atoms and thus decreases the 4− charge of N_2 inferred above from the population of π_v^* and π_σ^*. The interaction of the p_σ function with the zirconium atoms is weak due to orientation of this orbital perpendicular to the Zr–Zr axis.

Table 6 summarizes the atomic charges for the optimized model **I** and the corresponding p-orbital populations of dinitrogen, calculated by natural population analysis (NPA).

Table 6. NPA charges of model systems **I** and **III**; NPA s and p orbital populations of dinitrogen in **I** and **III**.

	Model **I** (D_{2h})				Model **III** (C_1)		
Atoms	Charge[a]	Orbital[b]	Charge[c]	Atoms	Charge[a]	Orbital[b]	Charge[c]
Zr	1.70	2s	1.69	Zr	1.68	2s	1.70
N	−0.91	$2p_x$	1.64	N	−0.94	$2p_x$	1.62
$N_{AD}H_2$[d]	−0.58	$2p_y$	1.04	$N_{AD}H_2$[d]	−0.54	$2p_y$	1.03
PH_3	0.18	$2p_z$	1.54	PH_3	0.17	$2p_z$	1.59

[a] Charge for each atom. [b] Orbitals from the nitrogen atom. [c] Population for each atomic orbital. [d] N_{AD} is the nitrogen atom of the NH_2^- group.

In agreement with the above orbital analysis, a large amount of charge density is transferred from the zirconium atoms to dinitrogen, which therefore is strongly reduced. As can be seen from Table 6 electron donation is almost equally distributed to π_h^* and π_v^*. However, due to charge donation from the amide donor orbitals and from the negatively charged dinitrogen ligand to the metal atoms, the +4 charge of the Zr atoms is reduced to +1.70, and the −4 charge on the N_2 ligand is reduced to −1.82, which is more compatible with formulation of the N_2 ligand in **3** as a diazenido(2−) moiety (N_2^{2-}). In contrast, the N–N bond length and stretching frequency seem to indicate that this complex is at the hydrazido (N_2^{4-}) stage, even though the N–N stretching frequency of **3** is lower than that of N_2H_4. This apparent discrepancy is explained by the fact that both the transfer of electron density from the metal atoms to the π* orbitals of dinitrogen and the donation from the π orbitals of dinitrogen to the metal atoms weaken the N–N bond and thus cause an increase in the N–N distance and a decrease in the N–N stretching frequency.

On the basis of molecular orbital theory, it was claimed that the end-on bridging mode with two medium-strength π interactions is generally preferred over the side-on bridging mode with one strong σ and one weak δ bond.[24] However, if one of the d orbitals of the metal atoms which form a π bond in the end-on case is blocked by strong p donors like amides, the side-on bridging mode becomes more favourable. Thus, the orientation of the amide lone pairs determines the bridging mode of the complex. In model **I**, the d_{xz} orbital must be blocked to make the side-on bridging mode favourable. Therefore, the amide lone pairs must be oriented parallel to the Zr–Zr axis. Our model **I** used for the DFT calculations exhibits this arrangement of amide lone pairs, but after geometry optimization the corresponding amide π donor orbitals ($N_{AD}(p)$, $b_{2g}\langle 51\rangle$) show no interaction with the d_{xz} functions of the metal atoms, as can be seen in Table 5 and Figure 8. In fact, the d_{xz}^+ orbital is blocked, but by amide σ donor functions forming the $N_{AD}\_d_{xz}^+$ orbital ($b_{2g}\langle 42\rangle$), as shown in Figure 8. The orientation of the amide lone pairs, however, becomes important in the bent Zr_2N_2 unit (see below).

Electronic structure of the bent μ-η^2:η^2 Zr_2N_2 core: In this section two optimized structures of the μ-η^2:η^2-N_2 system are presented in which the planar core can bend due to the application of lower symmetries, namely, C_{2v} (**II**) and C_1 (**III**). The experimental and calculated structures of **I**–**III** are compared in Table 4, and the optimized structures of **I** and **III** are presented in Figure 9. In C_{2v} symmetry (**II**), the Zr–N bond lengths do not change significantly with respect to **I**.

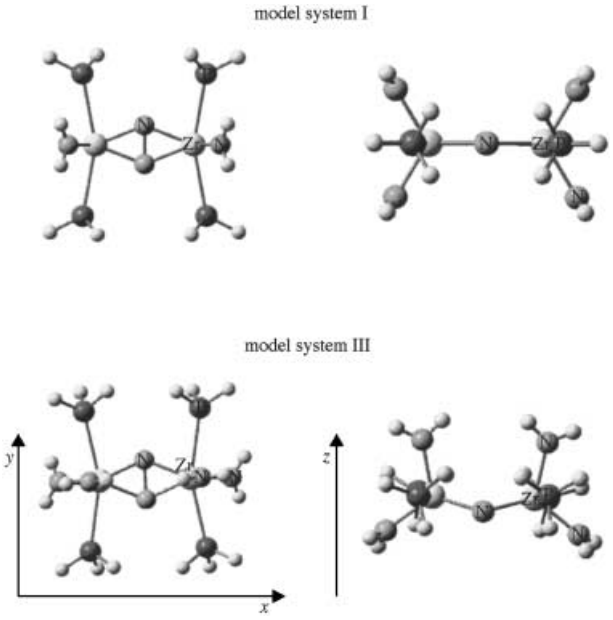

Figure 9. Structures of the optimized models **I** and **III**.

However, the Zr-N_2-Zr core bends slightly (Zr-N-N-Zr dihedral angle of 164.4°). The structure lies 1.2 kcal mol^{-1} below **I** (Table 4). Optimization in C_1 symmetry (**III**) leads to a more pronounced bending of the Zr-N_2-Zr core with a dihedral angle of 147.8°; the corresponding total energy is 11.2 kcal mol^{-1} below that of **I**. The N–N bond length increases from 1.57 Å in **I** to 1.63 Å in **III**. Importantly, the two amide lone pairs on top of the bent core have rotated by about 90° in **III**, so that they are now perpendicular to the Zr–Zr axis (see Figure 9). This rotation is forbidden in C_{2v} symmetry.

To understand the much lower energy of the bent structure, the electronic structure of model **III** must be considered in more detail. Contour plots of important molecular orbitals of **III** are shown in Figure 10; corresponding charge contributions are given in Table 7. The two amide lone pairs, which have rotated by about 90°, are now slightly mixed with the zirconium d functions (see Table 7), that is, the orbital

0947-6539/03/0902-0526 $ 20.00+.50/0 *Chem. Eur. J.* **2003**, *9*, No. 2

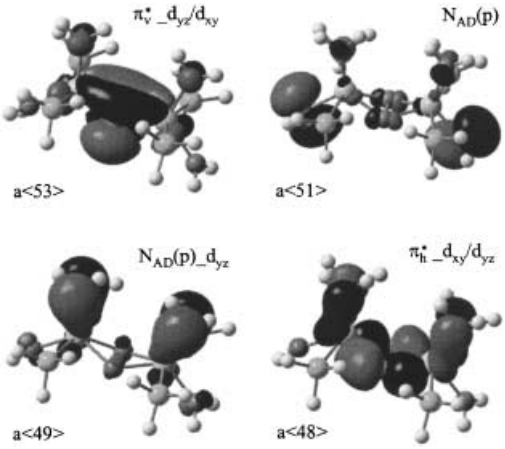

Figure 10. Contour plots of important molecular orbitals of **III**.

Table 7. Charge contributions of model **III**.[a]

Orbital	Label	Energy [Hartree]	Charge decomposition [%][b]				
			Zr	Zr d orbitals	N	P	N_{AD}[c]
d_{yz}/d_{xy}	a⟨54⟩	−0.00048	56	51	0	11	9
π_v^*_d_{yz}/d_{xy}	a⟨53⟩	−0.13156	22	21	67	2	8
$N_{AD}(p)$_d_{xy}	a⟨52⟩	−0.19692	11	7	13	6	69
$N_{AD}(p)$	a⟨51⟩	−0.20025	9	3	5	3	83
$N_{AD}(p)$_π_h^*_d_{xy}	a⟨50⟩	−0.20483	14	11	17	4	62
$N_{AD}(p)$_d_{yz}	a⟨49⟩	−0.21694	11	9	2	8	75
π_h^*_d_{xy}/d_{yz}	a⟨48⟩	−0.23252	28	26	41	4	24

[a] Only selected orbitals are listed. [b] If several equivalent atoms exist, the charge decomposition gives the sum of all contributions. [c] N_{AD} is the nitrogen atom of the NH_2^- group.

$N_{AD}(p)$_d_{yz}, which results from the two rotated amide lone pairs and the d_{yz} function of the metal, has 9 % metal d-orbital character. The HOMO is now derived from the mixed d_{yz}/d_{xy} orbitals together with the π_v^* function of dinitrogen (Figures 10 and 11). As can be seen from Figure 10, the former δ bond between the zirconium atoms and dinitrogen has become a pseudo π bond. The π_h^*_d_{xy}/d_{yz} orbital is also derived from a combination of the d_{xy} and d_{yz} functions of the metal atoms (Figures 10 and 11). Importantly, this orbital shows strong mixing with the rotated amide lone pairs (cf. Table 7). This leads to decreased zirconium and dinitrogen character of this orbital and weakening of the σ bond between the metal atoms and dinitrogen. On the other hand, the contribution of the amide lone pairs to this orbital is increased from 0 % (planar core) to 24 % (Table 7). These effects reduce the negative charge on the axial amido groups from −0.58 (planar) to −0.54 (bent; Table 6).

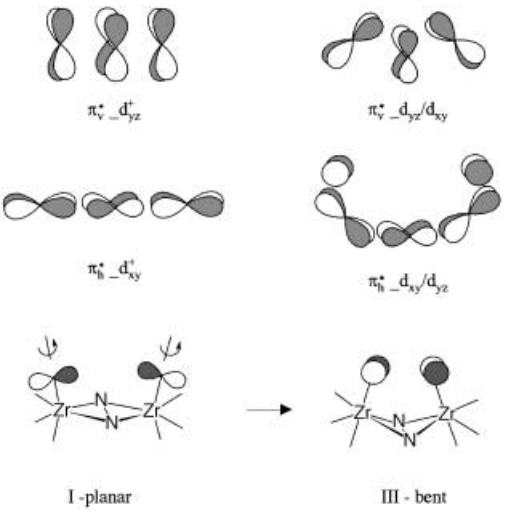

Figure 11. Effect of bending (**I** → **III**) on the MOs.

A comparison of frequencies of the Zr_2N_2 core for the models **I**–**III** derived from the DFT calculations is given in Table 8. Importantly, the frequency of the metal–metal stretch increases in **III** compared to **I** and **II**, whereas the other A_g mode (N–N stretch) is lower in frequency. This is due to the elongation of the N–N bond in **III** (see Table 4). The B_{1g} mode (not observed experimentally) shifts down to 627 cm^{-1} in **III**. The B_{2u} mode, which is split into two bands in the DFT calculations on **I** (see above), shows no mixing with ligand modes for the bent models **II** and **III**. The DFT calculations on these geometries predict the B_{2u} mode at 417 (**II**) and 445 cm^{-1} (**III**), with an isotope shift of about 10 cm^{-1} (Table 8). The B_{3u} mode is shifted to lower frequency in **II** and **III** compared to **I**.

Table 8. Comparison of the calculated (B3LYP) frequencies of the model systems **I**–**III**.

Mode[a]	**I** (D_{2h})		**II** (C_{2v})		**III** (C_1)	
	^{14}N [cm^{-1}]	^{15}N [cm^{-1}]	^{14}N [cm^{-1}]	^{15}N [cm^{-1}]	^{14}N [cm^{-1}]	^{15}N [cm^{-1}]
$A_g(1)$	262	261	266	265	305	301
$A_g(2)$	717	695	743	720	703	682
B_{1g}	685	667	689	671	627	607
B_{2u}	403	397	417	407	445	434
	313	310				
B_{2u}	780	757	770	747	746	725

[a] The labels refer to D_{2h} symmetry (model **I**). Modes of corresponding character are listed in columns C_{2v} (model **II**) and C_1 (model **III**).

Discussion

In the preceding sections the vibrational structure of the planar Zr_2N_2 core was defined, and the dependence of its electronic and vibrational structure on the equilibrium geometry (planar vs bent) explored. The Raman spectroscopic data complement earlier results obtained on the side-on N_2 bridged Zr_2 complexes **1** and **2**.[3, 5] In qualitative agreement with these results, the N–N stretching frequency of **3** is 775 cm^{-1}, with an isotope shift of −22 cm^{-1}. Further, the Raman peak at 295 cm^{-1} is identified as the Zr–Zr stretch (^{15}N shift: −1 cm^{-1}). This assignment is based on the high intensity of this Raman band and its appearance in many overtones and combination modes. The same applies to the N–N stretch, and this indicates that both vibrations of A_g symmetry are subject to pronounced Albrecht A-term resonance enhancement with respect to the $N_2 \rightarrow Zr$ CT transition at 670 nm. Moreover, these assignments are supported by DFT calculations, which predict the positions and ^{15}N isotope shifts of the N–N and metal-metal stretching vibrations to be at 717 cm^{-1}

($-22\ cm^{-1}$) and $262\ cm^{-1}$ ($-1\ cm^{-1}$), respectively. Based on these calculations and a normal coordinate analysis, the third Raman-active vibration of the planar ZrN_2 core, B_{1g}, is predicted to have a frequency of about $628\ cm^{-1}$, with a ^{15}N isotope shift of $19\ cm^{-1}$. No corresponding feature, however, could be identified in the Raman spectra. This is probably related to the fact that no excited-state distortion along the B_{1g} coordinate can be expected.

Infrared spectroscopic measurements on **3** further enabled the first experimental identification of the ungerade modes of the side-on Zr_2N_2 core. Based on these data, a quantum chemistry assisted normal coordinate analysis (QCA-NCA) was performed to generate an experimentally calibrated force field for the side-on N_2-bridged binuclear structure. In agreement with the DFT prediction of the B_{2u} vibration at $403\ cm^{-1}$ (isotope shift: $-6\ cm^{-1}$) and the B_{3u} vibration at $780\ cm^{-1}$ (isotope shift $-23\ cm^{-1}$), these modes are assigned to the bands at 690 and $441\ cm^{-1}$, which exhibit isotope shifts of -10 and $-13\ cm^{-1}$, respectively. The experimental isotope shift of the B_{3u} mode is much smaller than predicted theoretically, probably because this mode mixes with a vibration of the terminal ligands. As our model includes the terminal N and P ligands in the simplest approximation, this mixing is not reproduced in the DFT calculations or the NCA. Apart from this discrepancy, very good agreement between calculated and observed vibrational frequencies is achieved after NCA. The obtained force constants are $1.53\ mdyn\,Å^{-1}$ for N–N and $2.58\ mdyn\,Å^{-1}$ for Zr–N. This reflects the activation of dinitrogen in the complex relative to the free N_2 molecule ($22.42\ mdyn\,Å^{-1}$).[22] In fact, this force constant is much lower than that of free hydrazine ($4.3\ mdyn\,Å^{-1}$).[23]

The overall description of the electronic structure of the planar Zr_2N_2 core is compatible with that reported earlier.[24] Zirconium–dinitrogen bonding is dominated by σ bonding, which is mediated by the doubly occupied in-plane π* orbital π_h^*. The out-of plane N_2 orbital π_v^* is involved in a δ bond between the metal atoms and dinitrogen. According to a concept developed earlier, end-on binding of N_2 should be preferred over side-on bonding in early transition metal dinitrogen complexes.[24] Based on comparative DFT calculations on titanium and zirconium N_2 complexes, we find that this is only true for Ti: whereas an end-on N_2 complex of Ti is $11.9\ kcal\,mol^{-1}$ more stable than its side-on counterpart, an end-on N_2 complex of Zr is $+3.1\ kcal\,mol^{-1}$ less stable than the side-on N_2 complex **3** (all models have terminal PH_3/NH_2 ligation analogous to model **III** and were optimized in C_1 symmetry). The obvious reason for this difference in reactivity is orbital overlap: due to the more diffuse wavefunctions in Zr as compared to Ti and the long N–N bond length, side-on bonding of N_2 is more favourable for Zr than for Ti. It has been reported that the coordination mode of N_2 is further influenced by the orientation of the lone pairs of the axial ligands: if these lone pairs are oriented along the metal–metal axis, one of the metal d orbitals necessary for end-on binding of N_2 is blocked by a π interaction, and side-on bonding of N_2 occurs.[24] Instead of such a π interaction between metal atom and amide, we find a corresponding σ interaction which, however, has the same consequences. Nevertheless, the orientation of the amide lone pairs relative to the Zr–Zr axis is found to be critically important with respect to bending of the planar Zr_2N_2 core towards a butterfly-distorted geometry: if rotation of the amide lone pairs away from the Zr–Zr axis is disabled, the core basically stays planar. This is shown by the DFT optimization in C_{2v} symmetry, which allows bending of the core but not rotation of the axial amido groups. In this case only a slight bending of the core is observed (model **II**). The driving force for this small distortion in the C_{2v} calculation is not clear; the corresponding energy gain with respect to the planar core (D_{2h} symmetry) is very small ($1.2\ kcal\,mol^{-1}$). In the real compound **3**, rotation of the amide lone pairs is prevented by the macrocyclic structure of the terminal ligands, and a planar core is in fact observed.

Remarkably, however, if the vertical mirror plane containing the Zr–Zr axis is removed, the terminal amido groups rotate by 90° and become oriented perpendicular to the Zr–Zr direction. This structural change now causes a pronounced bending of the Zr_2N_2 core (dihedral angle 147.8°) and a marked decrease in total energy ($-11.2\ kcal\,mol^{-1}$). There are two major electronic-structural consequences of this distortion: 1) the lone pairs of the amido groups on top of the bent Zr_2N_2 core mix with the in-plane N_2 π_h^* orbital via a metal hybrid orbital derived from d_{xy}/d_{xz} (π_{h-}^* d_{xy}/d_{yz}, $a\langle 48\rangle$); 2) the other hybrid orbital of the metal d_{xy}/d_{yz} orbitals forms a pseudo π bond with the out-of-plane π_v^* orbital of the bridging dinitrogen (π_{v-}^* d_{yz}/d_{xy}, $a\langle 53\rangle$) (Figures 10, 11 and Table 7). This way, the σ-bonding interaction between the metal atoms and π_h^* is weakened, but the interaction between the metal atoms and π_v^* is increased. Overall, this leads to a stronger interaction between the amide lone pairs and the Zr_2N_2 core and a more uniform distribution of electron density between the metal atoms and N_2 (in the planar structure there is a very strong metal–ligand σ interaction through π_h^* and a very weak δ interaction through π_v^*, see above). These findings are in qualitative agreement with the earlier hypothesis that bending of the Zr_2N_2 core allows a more pronounced delocalization of the electron density of the N_2 ligand (the fact that we find a stabilization of the bent model **III** with respect to the planar structure **I** of $-11.2\ kcal\,mol^{-1}$, whereas in the literature an energy gain of $-24.4\ kcal\,mol^{-1}$ is given, is due to a different choice of basis set).[16]

While rotation of the amido groups is prevented in the planar Zr_2N_2 unit of **3** by the terminal P_2N_2 ligands, there is one side-on N_2 bridged Zr_2 complex with two phenolate ligands on top of a bent Zr_2N_2 core, namely, $[\{(PNP)Zr(OAr)\}_2(\mu\text{-}\eta^2\text{:}\eta^2\text{-}N_2)]$ (**2**; Scheme 1). The orientation of the phenolate lone pairs in this structure is intermediate between parallel and perpendicular to the Zr–Zr direction. It remains to be investigated whether rotation of the phenolate lone pairs to a position perpendicular to Zr–Zr, the minimum energy position according to the above calculations, is hindered by steric restrictions in this compound. Interestingly, the Raman spectrum of **2** shows one additional peak at $595\ cm^{-1}$ with a ^{15}N isotope shift of $-19\ cm^{-1}$.[5] The frequency and isotope shift of this peak would fit to our theoretical prediction of the B_{1g} mode frequency of the Zr_2N_2 unit: while the DFT calculations of the planar core predicts the B_{1g} mode to be at $685\ cm^{-1}$ (isotope shift: $-18\ cm^{-1}$), bending of the

0947-6539/03/0902-0528 $ 20.00+.50/0 *Chem. Eur. J.* **2003**, *9*, No. 2

core shifts the calculated frequency of the B_{1g} mode to 627 cm^{-1} (isotope shift: -20 cm^{-1}, see Table 8). Because the NCA calculation on the planar core predicts the B_{1g} mode to be about 60 cm^{-1} lower than the DFT calculation (cf Table 2), the theoretical prediction of the B_{1g} frequency of the bent core should be lowered by this amount as well, leading to an expected frequency of about 570 cm^{-1}. This prediction would fit to the observed position of the Raman peak at 595 cm^{-1}. It is, however, still unclear how this mode obtains Raman intensity, as also in the butterfly-distorted geometry no excited-state distortion along the B_{1g} coordinate is conceivable.

In summary, a complete understanding of the vibrational and electronic structure of the planar Zr_2N_2 core has been achieved, and the electronic-structural driving force for bending of this core towards a butterfly structure has been analyzed. Further spectroscopic studies on bent μ-η^2:η^2-N_2 complexes should allow the theoretical conclusions regarding the influence of terminal ligands on the equilibrium geometry of the Zr_2N_2 core and the appearance of the B_{1g} vibration in the distorted geometry to be checked.

Experimental Section

IR Spectroscopy: Middle-infrared (MIR) spectra were obtained from RbI pellets on a Mattson Genesis Typ I spectrometer. Far-infrared (FIR) spectra were obtained from RbI pellets on a Bruker IFS 66 FTIR spectrometer. Both instruments were equipped with a Cryogenics helium cryostat. The spectra were recorded at 10 K and the resolution was set to 2 cm^{-1}.

Resonance Raman spectroscopy: Resonance Raman spectra were measured on a Dilor XY Raman spectrograph with triple monochromator and CCD detector. An Ar/Kr mixed-gas laser with a maximum power of 5 W was used for excitation. Spectra with excitation wavelengths of 454.5, 488.0, 514.5, 568.2 and 647.1 nm were recorded. Maximum resonance enhancement was found for an excitation wavelength of 647.1 nm. The spectra were measured on RbI pellets cooled to 10 K with a helium cryostat. The spectral bandpass was set to 2 cm^{-1}.

UV/Vis spectroscopy: Optical absorption spectra were obtained from KBr pellets. The spectra were recorded at 10 K on a Varian Cary 5 UV/Vis/NIR spectrometer.

Normal coordinate analysis: Normal coordinate calculations were performed with the QCPE computer program 576.[25] The calculations were based on a general valence force field, and the force constants were refined by using the nonlinear optimization routine of the simplex algorithm according to Nelder and Mead.[26] Only selected force constants were refined due to the QCA-NCA procedure. The QCA-NCA procedure is useful for the treatment of large molecules. If the real molecule is too large to be handled with ab initio theory, a simplification is necessary. In the case of complex **3**, the $[P_2N_2]$ ligands were substituted by PH_3 and NH_2^-. This leads to model **I**, which is suitable for DFT calculations. Frequencies and force constants (f matrix) of this model were calculated. To remove artificial interactions and to allow easier handling, the H atoms of the PH_3 and NH_2^- ligands were removed to give the model $([P_2N_2]Zr)_2(\mu$-η^2:η^2-$N_2)$. The f′ matrix, obtained by truncation of the complete matrix f, can formally be divided into two parts: the force constants of the Zr_2N_2 unit (core), which are fitted to experimental frequencies, and the force constants of the ZrN and ZrP parts (frame), which are of no further interest. By neglecting small interactions it is possible to describe the core by only a few force constants. The force constants of the frame and nondiagonal elements between frame and core were fixed at their theoretical values. Thus, only selected force constants were refined in the QCA-NCA procedure.

DFT Calculations: Spin-restricted DFT calculations using the Becke three-parameter hybrid functional with the correlation functional of Lee, Yang and Parr (B3LYP)[27–29] were performed for the singlet ground state of simplified models of complex **3** and analogous Zr end-on and Ti side-on/end-on structures. The LanL2DZ basis set was used for the calculations. It applies Dunning/Huzinaga full double-zeta (D95) basis functions[30] on first-row atoms and Los Alamos effective core potentials plus DZ functions on all other atoms.[31, 32] Charges were analyzed by using the natural bond orbital (NBO) formalism.[33–36] All computational procedures were used as implemented in the Gaussian 98 package.[37] Wavefunctions were plotted with the visualization program Gaussview 2.1. The force constants in internal coordinates were extracted from the Gaussian output by using the program Redong.[38]

Acknowledgements

F.T. thanks the state of Schleswig-Holstein and the FCI (Fonds der Chemischen Industrie) for financial support. F.S. thanks U. Cornelissen for help with the spectroscopic measurements. M.D.F. thanks NSERC of Canada for a research grant.

[1] M. D. Fryzuk, S. A. Johnson, *Coord. Chem. Rev.* **2000**, *200*, 379.
[2] F. Tuczek, N. Lehnert, *Angew. Chem.* **1998**, *110*, 2780; *Angew. Chem. Int. Ed.* **1998**, *37*, 2636.
[3] J. D. Cohen, M. Mylvaganam, M. D. Fryzuk, T. M. Loehr, *J. Am. Chem. Soc.* **1994**, *116*, 9529.
[4] M. D. Fryzuk, T. S. Haddad, S. J. Rettig, *J. Am. Chem. Soc.* **1990**, *112*, 8185.
[5] J. D. Cohen, M. D. Fryzuk, T. M. Loehr, M. Mylvaganam, S. J. Rettig, *Inorg. Chem.* **1998**, *37*, 112.
[6] R. Duchateau, S. Gambarotta, N. Beydoun, C. Bensimon, *J. Am. Chem. Soc.* **1991**, *113*, 8986.
[7] B. E. Wiesler, Ph.D. thesis, Johannes Gutenberg-Universität Mainz (Germany), **1999**.
[8] W. J. Evans, T. A. Ulibarri, J. W. Ziller, *J. Am. Chem. Soc.* **1988**, *110*, 6877.
[9] P. Roussel, P. Scott, *J. Am. Chem. Soc.* **1998**, *120*, 5836.
[10] P. Roussel, W. Erington, N. Kaltsoyannis, P. Scott, *J. Organomet. Chem.* **2001**, *635*, 69.
[11] J. Guan, T. Dubé, S. Gambarotta, G. P. A. Yap, *Organometallics* **2000**, *19*, 4820.
[12] F. G. N. Cloke, P. B. Hitchcock, *J. Am. Chem. Soc.* **2002**, *124*, 9352.
[13] W. J. Evans, N. T. Allen, J. W. Ziller, *J. Am. Chem. Soc.* **2001**, *123*, 7927.
[14] P. J. Chirik, L. M. Henling, J. E. Bercaw, *Organometallics* **2001**, *20*, 534.
[15] M. D. Fryzuk, J. B. Love, S. J. Rettig, V. G. Young, *Science* **1997**, *275*, 1445.
[16] H. Basch, D. G. Musaev, K. Morokuma, *J. Am. Chem. Soc.* **1999**, *121*, 5754.
[17] H. Basch, D. G. Musaev, K. Morokuma, M. D. Fryzuk, J. B. Love, W. W. Seidel, A. Albinati, T. F. Koetzle, W. T. Klooster, S. A. Mason, J. Eckert, *J. Am. Chem. Soc.* **1999**, *121*, 523.
[18] N. Lehnert, F. Tuczek, *Inorg. Chem.* **1999**, *38*, 1671.
[19] The sixth mode is an ungerade butterfly mode which is low in intensity and frequency and is therefore normally not found in the infrared spectra.
[20] J. Tang, A. C. Albrecht in *Raman Spectroscopy*, *Vol. 2* (Ed.: H. A. Szymanski), Plenum Press, New York, **1970**.
[21] A. C. Albrecht, *J. Chem. Phys.* **1961**, *34*, 1476.
[22] A. Fadini, Molekülkraftkonstanten—Zur Theorie und Berechnung der Konstanten der potentiellen Energie der Moleküle, Steinkopff Verlag, Darmstadt, **1976**.
[23] E. Catalano, R. H. Sanborn, J. W. Frazer, *J. Chem. Phys.* **1963**, *38*, 2265.
[24] M. D. Fryzuk, T. S. Haddad, M. Mylvaganam, D. H. McConville, S. J. Rettig, *J. Am. Chem. Soc.* **1993**, *115*, 2782.
[25] M. R. Peterson, D. F. McIntosh, QCPE program 576, Quantum Chemistry Program Exchange, Department of Chemistry, Indiana University, Bloomington (USA), **1988**.
[26] J. A. Nelder, R. Mead, *Comput. J.* **1965**, *7*, 308.
[27] A. D. Becke, *Phys. Rev. A* **1988**, *38*, 3098.

  0947-6539/03/0902-0529 $ 20.00+.50/0

[28] A. D. Becke, *J. Chem. Phys.* **1993**, *98*, 1372.
[29] A. D. Becke, *J. Chem. Phys.* **1993**, *98*, 5648.
[30] T. H. Dunning, Jr., P. J. Hay in *Modern Theoretical Chemistry* (ed.: H. F. Schaefer III), Plenum, New York, **1976**.
[31] P. J. Hay, W. R. Wadt, *J. Chem. Phys.* **1985**, *82*, 270 and 299.
[32] W. R. Wadt, P. J. Hay, *J. Chem. Phys.* **1985**, *82*, 284.
[33] J. P. Foster, F. Weinhold, *J. Am. Chem. Soc.* **1980**, *102*, 7211.
[34] A. B. Rives, F. Weinhold, *Int. J. Quantum Chem. Symp.* **1980**, *14*, 201.
[35] A. E. Reed, R. B. Weinstock, F. Weinhold, *J. Chem. Phys.* **1985**, *83*, 735.
[36] A. E. Reed, L. A. Curtiss, F. Weinhold, *Chem. Rev.* **1988**, *88*, 899.
[37] M. J. Frisch, G. W. Trucks, H. B. Schlegel, G. E. Scuseria, M. A. Robb, J. R. Cheeseman, V. G. Zakrzewski, J. A. Montgomery, Jr., R. E. Stratmann, J. C. Burant, S. Dapprich, J. M. Millam, A. D. Daniels, K. N. Kudin, M. C. Strain, O. Farkas, J. Tomasi, V. Barone, M. Cossi, R. Cammi, B. Mennucci, C. Pomelli, C. Adamo, S. Clifford, J. Ochterski, G. A. Petersson, P. Y. Ayala, Q. Cui, K. Morokuma, P. Salvador, J. J. Dannenberg, D. K. Malick, A. D. Rabuck, K. Raghavachari, J. B. Foresman, J. Cioslowski, J. V. Ortiz, A. G. Baboul, B. B. Stefanov, G. Liu, A. Liashenko, P. Piskorz, I. Komaromi, R. Gomperts, R. L. Martin, D. J. Fox, T. Keith, M. A. Al-Laham, C. Y. Peng, A. Nanayakkara, M. Challacombe, P. M. W. Gill, B. Johnson, W. Chen, M. W. Wong, J. L. Andres, C. Gonzalez, M. Head-Gordon, E. S. Replogle, J. A. Pople, Gaussian 98, Rev. A.11, Gaussian, Inc., Pittsburgh, **2001**.
[38] A. Allouche, J. Pourcin, *Spectrochim. Acta* **1993**, *49A*, 571.

Received: August 9, 2002 [F4331]

  0947-6539/03/0902-0530 $ 20.00+.50/0